Correlation between the nanocrystalline Sm(Fe,Mo)12 and its out of equilibrium phase Sm(Fe,Mo)10

S Khazzan, L Bessais, G van Tendeloo, N Mliki

Correlation between the nanocrystalline $Sm(Fe,Mo)_{12}$ and its out of equilibrium phase $Sm(Fe,Mo)_{10}$

S. Khazzan,[1,2] L. Bessais,[1] G. Van Tendeloo,[3] and N. Mliki[2]
[1)] *CMTR, ICMPE, UMR7182, CNRS − Université Paris Est, 2-8 rue Henri Dunant F-94320 Thiais, France*
[2)] *Laboratoire Matériaux Organisation et Propriétés, Faculté des Sciences de Tunis, Université de Tunis El Manar, 2092 Tunis, Tunisie*
[3)] *EMAT, University of Antwerp, B-2020 Antwerp, Belgium*

Nanostructured Sm-Fe-Mo semi-hard magnetic material exhibiting enhanced magnetic properties can be produced by ball milling followed by recrystallization. Milled samples were annealed for 30 min in a vacuum at different temperatures (T_A) between 700 and 1190 °C. The effects of heat treatment and Mo content on structural and magnetic property changes have been investigated by means of x-ray diffraction using the Rietveld method, transmission electron microscopy and magnetic measurements. For samples annealed at $T_A > 900$ °C the tetragonal $ThMn_{12}$-type structure is identified, while for $700 < T_A < 900$ °C a new out of equilibrium $P6/mmm$ type structure was found as the major phase. This novel nanocrystalline phase has never been synthesized before. The correspondent stoichiometry is determined on the basis of the vacancy model. The Rietveld analysis gives a stoichiometry ratio equal to 1:10, for the out of equilibrium hexagonal phase, which is described with three crystallographic transition metal sites: $3g$ is fully occupied, $6l$ occupation is limited to hexagons surrounding the Fe dumbbell pairs $2e$. We have performed a magnetic and structural study of nanocrystalline metastable $P6/mmm$ $Sm(Fe_{1-x}Mo_x)_{10}$, correlated to structural transformation towards its equilibrium derivative $I4/mmm$ $Sm(Fe_{1-x}Mo_x)_{12}$. A maximum of the coercive field H_C ($H_C > 5$ kOe) has been observed for the new hexagonal $P6/mmm$ phase suggesting that nanocrystalline $Sm(Fe,Mo)_{10}$, is a semi-hard material, and is potential candidate for magnetic recording.

PACS numbers: 75.50.Bb, 75.50.Tt, 76.80.+y
Keywords: A. Rare-earth intermetallics; B. Magnetic property; C. Mechanical alloying and milling; F. Diffraction, Electron microscopy transmission; G. Magnetic application

I. INTRODUCTION

Magnetic nanoparticles receive significant attention according to their novel magnetic properties and potential technological applications. Rare earth transition metal intermetallic compounds (R−T) with magnetocrystalline anisotropy are suitable systems for the study of the finite size effects[1].

The binary phase RFe_{12} does not exist for all R elements. The $ThMn_{12}$ structure, however, can be stabilized by adding a third element M like Ti, Si, W[2–5], Mo[6], Cr[7] , V[8] or Al[9]. These systems are commonly synthesized by the conventional melting method[10]. Few studies though have been devoted to the Sm−Fe−Mo alloy.

Among the processes available for preparing nanomaterials, the techniques of melt-spinning, sputtering or high-energy milling with subsequent annealing, are the most currently used. These techniques usually lead to out-of-equilibrium nanocrystalline phases which still need thorough investigations.

In searching for Fe− rich rare earth intermetallic compounds suitable for permanent magnet fabrication, the RFe_{12} compounds have shown to be worth investigating further[2,8,11–13]. These intermetallic compounds retain the tetragonal $ThMn_{12}$ structure type (space group $I4/mmm$). The rare-earth atoms occupy the single $2a$ sites, while the transition metals Fe and M occupy the three sites: $8i$, $8j$, and $8f$.

The stoichiometric RT_5 structure of $CaCu_5$ $P6/mmm$ type can evolve to nonstoichiometric $P6/mmm$ structures. Atomic ordering generates phases with composition 2/17, 3/29, and 1/12. Their out of equilibrium precursor phases are found to adopt a $P6/mmm$ structure. These are generally described as having $TbCu_7$ type structure, except the $P6/mmm$ $Sm(Fe,Mo)_9$ phase, which we reported as the parent phase of $Sm_2(Fe,Mo)_{17}$[14]. To our acknowledge, no one has invoked the compound where Fe is substituted by Mo. Additionally, when two dumbbell pairs (T-T) substitute for 2R atoms over a $4RT_5$-type cell, the $ThMn_{12}$-type phase occurs as follows:

$$4(RT_5) - 2R + 4T\ (\text{dumbbell}) \longrightarrow 2(RT_{12})$$

The mechanical processing technique has been successfully used in the synthesis of numerous nanosized materials. The high energy ball milling with subsequent annealing, appears to be particularly convenient for the Sm-based alloys since samarium is extremely volatile. This process presents the advantage to assume better control of the stoichiometry of the materials as it is implemented in the solid state, well below the melting temperature. Furthermore it can provides large homogeneous batches of material. Heat treatment produces the formation of out-of-equilibrium phases stable up to high temperatures. The out-of-equilibrium phases are a precursor of the well known equilibrium phases[15,16] and are able to promote

intrinsic and extrinsic magnetic properties more promising than those obtained with the equilibrium phases.

Due to the induced plastic deformation, high energy ball milling may result in solid state alloying producing in-situ metastable structures, depending on the thermodynamics of the system. The inter-diffusion reaction to form alloys often needs further heat treatment[17–19].

Here, we propose to investigate the effect of thermal treatment on the coercivity of the semi-hard nanocrystalline $Sm(Fe,Mo)_{12}$ and $Sm(Fe,Mo)_{10}$ alloys, obtained after mechanical milling and subsequent annealing of the elemental powders. A structural study gives the stoichiometry and morphology of the new out-of-equilibrium and the equilibrium phase as well as the crystallographic parameters. The Curie temperature (T_C) evolution attests for the pertinence of the Fe substitution. Moreover, we show the dependence of the intrinsic magnetic properties on the molybdenum concentration and the recurrent coercivity.

II. EXPERIMENT

Various alloys with nominal composition $SmFe_{12-x}Mo_x$ ($x = 0.8$, 1, 1.5 and 2) have been prepared by mechanical alloying. The study of this series has been limited to $x \leq 2$ where the easy direction of magnetization of the tetragonal phase remains axial[20].

A mixture of high-purity powders of Sm (99.99%), Mo (99.8%) and prealloyed Sm_2Fe_{17} were milled in steel vials hermetically sealed in an argon filled glove box with O_2 and H_2O rate of 1 ppm.

The high energy ball milling process was performed in a Fritsch planetary ball mill (Pulverisette P7) with five steel balls of 15 mm for 5 h. The rotational speed of the vial and the disk were 1500 tr/min and 600 tr/min respectively. The powders were subsequently heat treated for 30 min at a temperature between 700 °C and 1190 °C.

The structure was studied by means of a Bruker X-ray diffractometer with automatic divergence slit (CuKα radiation $\lambda = 1.54178$ Å). The refinement of X-ray diffraction (XRD) patterns was carried out using the FULLPROFF code based on the Rietveld technique. The Rietveld method was used to analyze the crystal structures and to calculate the lattice parameters, the diffraction domain size and strain rate. The weight percentage of each of the coexisting phases is directly obtained with the approximation of a Brindley absorption factor equal to 1. Isotropic Lorentzian and Gaussian contribution of size and micro-strains were taken into account. The full-width-at-half-maximum of the Gaussian H_G and Lorentzian H_L component of the profile function are given by :

$$H_G^2 = u\tan^2\theta + v\tan\theta + w$$

$$H_L = \zeta\tan\theta + \frac{\xi}{\cos\theta}$$

ξ leads to the auto-coherent domain size by means of the Scherrer equation. The u parameter leads to an estimate of the isotropic broadening due to strain effects. The various structural parameters: X, Z atomic positions, Debye-Waller factor and occupancy parameter s, cell parameters and the u and ξ profile parameters were least-square fitted. The "goodness-of-fit" indicator R_B is calculated as follows[21–23]:

$$R_B = \frac{\sum_K |I_K(o) - I_K(c)|}{\sum_K I_K(o)}$$

$I_K(o)$ is the observed Bragg intensity and $I_K(c)$ is the calculated one.

In order to explore the samples microstructure, transmission electron microscopy was performed on a CM20 microscope operating at 200 kV, with a LaB_6 source. Thin specimens were prepared as follows: after embedding specimen powder in a thin layer of resin, the mixture is kept out drying. Then, some pieces are cut and pasted on a copper slot with the same resin. Finally, the samples are thinned to electron transparency by Ar-ion milling from both sides till a hole in the specimen center is generated. By this method, a large number electron transparent plate-like crystallites were obtained.

The magnetization has been measured using a Physical Properties Measurement System PPMS9T Quantum design equipment and a maximum applied field of 90 kOe on sample in epoxy resin.

The Curie temperatures were measured with a DSM-8 MANICS magnetometer/susceptometer. The sample is sealed in silica tubes to avoid oxidation upon heating. It is then fixed at the end of a brass rod and placed in the presence of an external magnetic field gradient perpendicular to the rod. A magneto-optic device detects the force by measuring the torsion angle of a wire. Then, a servo-controlled device applies a compensation force that brings the sample rod back into its initial position. Thermomagnetic data are measured under an applied field of 0.1 T and a heating rate of 5K/min. Curie temperatures T_C are determined from the $M-T$ curves by extrapolating the linear part of the $M-T$ curve and finding the temperature values of the intersection with the extended baseline.

III. RESULTS

A. Crystallographic analysis

In this section, we intend to probe the effect of thermal treatment on phase formation. Structural investigations of various alloys with nominal composition ($0.8 \leq x \leq 2$) have been carried out. Figure 1 illustrates the XRD of the as milled powder. It is clearly seen that the mixture consists of (Sm,Mo) in a quasi amorphous state besides

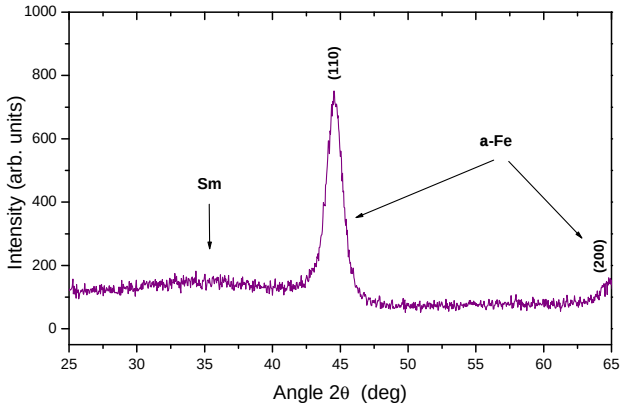

FIG. 1. XRD pattern of the as milled $Sm(FeMo)_{12}$ powder.

two broadened peaks (110) and (200) of $\alpha-$Fe. No alloy formation occurs. It is necessary to anneal the as milled powder in order to crystallize the material. To reach this purpose, optimization of thermal treatment conditions must be undertaken. The powders, wrapped in a tantalum foil, were annealed under vacuum for 30 min at different temperatures.

As an example, one can see on figure 2, the XRD diagrams of the annealed material at temperatures T_A = 700, 850 and 1190 °C. At T_A = 700°C, the diagram is representative of unambiguous hexagonal $P6/mmm$ cell of the $CaCu_5$ type, as the main phase. This is in agreement with the results obtained for mechanically alloyed $SmFe_{11}Ti$[24] samples.

For the samples annealed at T_A = 1190 °C, the XRD shows a full transformation of the alloy into the typical $ThMn_{12}$ structure type with the expected intensities of the (002) and (202) superstructure extra lines of the $I4/mmm$ space group. Moreover, with increasing annealing temperature, the broadening of the diffraction peaks reduces which indicates a better crystallinity at high temperature.

The XRD pattern for the samples annealed at T_A = 850 °C shows a gradual merging of the (002) and (202) superstructure extra lines, the two phases $I4/mmm$ and $P6/mmm$ coexist (Fig. 2).

In the $SmFe_{12-x}Mo_x$ compounds, the Fe atoms occupy three crystallographic non-equivalent sites, denoted Fe(8i), Fe(8j) and Fe(8f) (Fig. 3).

In the Rietveld refinement, the different parameters were independently varied.

First, the refinement was performed with Mo statistically distributed among all crystallographic sites. However, the agreement was improved with Mo atoms distributed on 8i sites as observed for bulk material[25–27]. Indeed, Hu *et al.*[27] have deduced from neutron diffraction that Mo atoms prefer the 8i sites in $YFe_{12-x}Mo_x$.

Figure 4 shows the Rietveld refinement for the $SmFe_{11}Mo$ (x = 1) compound annealed at 1190°C. Additional weak lines are assigned to a small amount of SmO-N, Sm_2O_3 and SmO_6. The results concerning the

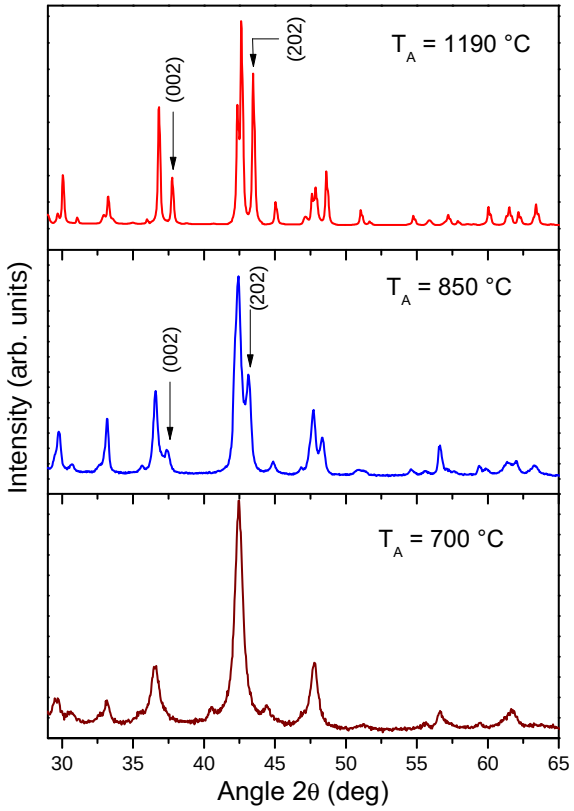

FIG. 2. XRD pattern evolution of $SmFe_{10.5}Mo_{1.5}$ annealed at different temperatures.

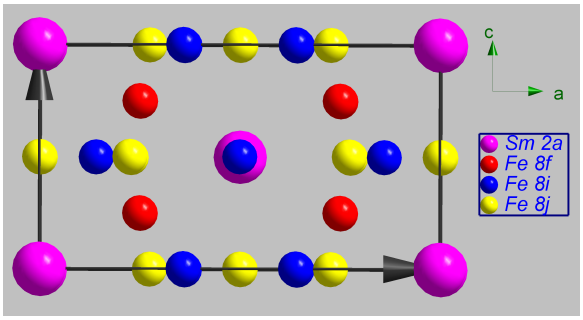

FIG. 3. The crystal structure of the tetragonal $ThMn_{12}$ phase.

fit of the various samples are presented in table I.

It appears that the unit cell parameters a and c increase with increasing x. However, the c/a ratio does not depend on x, indicating an isotropic expansion of the lattice after Mo substitution. The unit cell volume almost linearly increases with Mo increment. The small trend of an increase of the diffraction domain size as the Mo content increases is consistent with the disorder brought by the third element slowing down the diffusion process.

The crystallographic analysis of the hexagonal phase, for T_A < 800 °C, is more complex than that for the tetragonal phase. The understanding of the structure

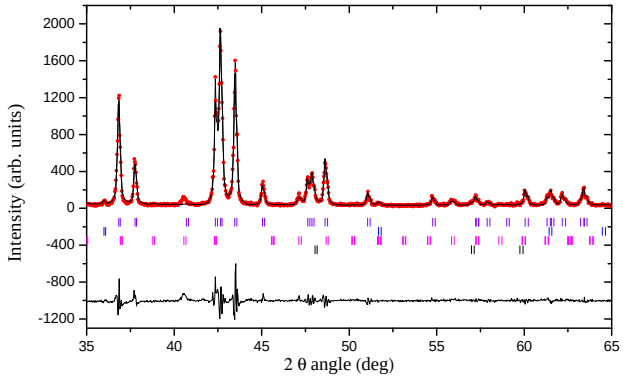

FIG. 4. Rietveld analysis for the tetragonal $SmFe_{11}Mo$ annealed 1190°C.

TABLE I. Crystallographic parameters from a Rietveld refinement of $SmFe_{12-x}Mo_x$ annealed at 1190°C. a and c are unit cell parameters, V unit cell volume, D auto-coherent domain size, χ^2, R_B agreement factors.

	$x=1$	$x=1.5$	$x=2$
a (Å)	8.548	8.561	8.569
c (Å)	4.772	4.783	4.792
c/a	0.558	0.558	0.559
V (Å^3)	349	351	352
$x\{8i\}$	0.359	0.359	0.358
$x\{8j\}$	0.273	0.275	0.278
D (nm)	60	63	65
χ^2	1.89	3.08	6.22
R_B	4.40	2.48	5.46

transformation is still open to discussion since no accurate information is given until now about the 1/12 precursor. Q.F. Xiao *et al.* and Z.X. Tang *et al.* have shown that this metastable phase can be described as a $TbCu_7$ type structure[4,28].

Teresiak *et al.*[29] have also presented the 2/17 out of equilibrium precursor as having the 1/7 type structure. However, in a previous work[14,30], we have shown that the 2/17 out of equilibrium phase is rather of 1/9 type structure. Then, starting from two independent equilibrium phases (2/17 and 1/12) one may expect a new metastable phase for the 1/12 phase. The precursor-structure has been refined on the basis of the vacancy model, previously proposed for over-stoichiometric Sm-Co based compounds[31]. This model, governed by the s Sm vacancy rate[24,32,33] (table II) , was revisited and generalized for a large s values (s up to 0.5)[30,34]. The deviation from the stoichiometry is represented by the $R_{1-s}T_{5+2s}$ formula.

The R atoms occupy the Wyckoff position $1a$ (0,0,0) of the hexagonal $P6/mmm$ structure (figure 5). These R atoms are partially substituted by $2s$ T atoms, known as the dumbbell pairs that occupy the $2e$ site (0,0,z). Due to the presence of the vacant R position, a part of the neighboring $2c$ T atoms in positions $(\frac{1}{3}, \frac{2}{3}, 0)$ move

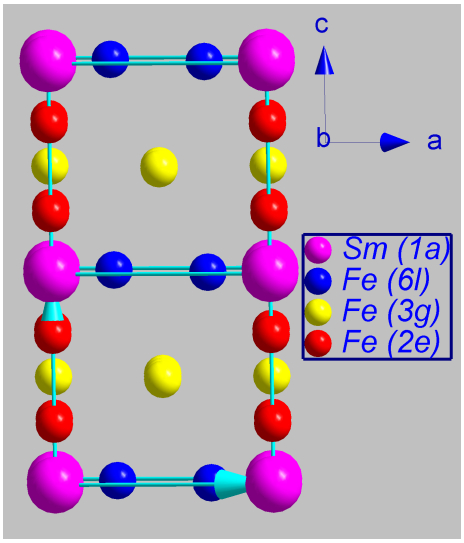

FIG. 5. The crystal structure of the hexagonal $P6/mmm$ phase.

towards the R vacancy, along the c-axis, occupying then the positions $6l$ $(x, 2x, 0); (x < \frac{1}{3})$ for which the atom number is equal to $6s$.

The remaining $2(1-3s)$ T atoms, are located in the $2c$ position while those T at the $3g$ site $(\frac{1}{2}, 0, \frac{1}{2})$ are not disturbed and fully occupied. It must be outlined that for $s = 0.33$, the $2c$ atoms do not exist anymore and hence $6s = 2$ (Table II).

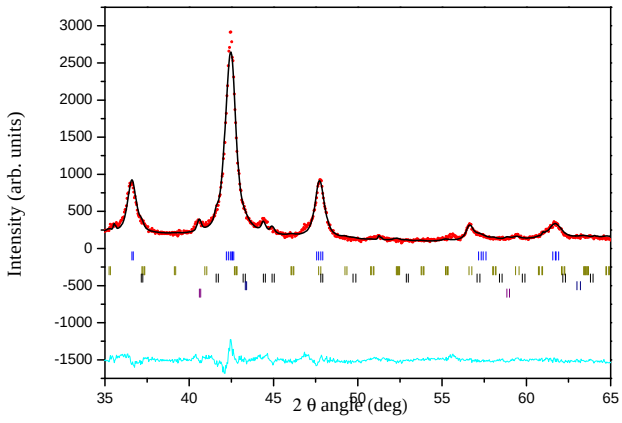

FIG. 6. Rietveld analysis for the hexagonal $SmFe_9Mo$ annealed at 750°C.

According to the vacancy model the $TbCu_7$ (s=0.22) stoichiometry differs from the $CaCu_5$ (s=0) one by the s value. So, only Sm($1a$) occupancy is involved. In their works, Teresiak *et al.* [29,35] have invoked a modified $TbCu_7$ structure which does not match the general formula of $R_{1-s}T_{5+2s}$. On one hand, Sm($1a$) occupancy varies from s=0.65 up to 0.78. As an example, for s= 0.65 value the R atom percentage is about 5% while in 1/7 stoichiometry is much higher (12.5%). On the other

TABLE II. Atom Wyckoff positions, number of subsequent atom in the $R_{1-s}T_{5+2s}$ hexagonal $P6/mmm$ structure as a function of the s parameter atom occupancy and Wyckoff positions with number of subsequent atom in the RT_{12} $I4/mmm$ tetragonal structure.

Atom position	$R_{1-s}T_{5+2s}$					Atom position	RT_{12}
	s=0	0<s<0.33	s = 0.22	s >0.33	s = 0.42		
	$CaCu_5$		$TbCu_7$		1/10		
Sm (1a) 0,0,0	1	1-s	0.78	1-s	0.58	Sm (2a) 0,0,0	2
T_1 (2c) $\frac{1}{3},\frac{2}{3}$, 0	2	2(1-3s)	2	0	0	T_1 (8f) $\frac{1}{4},\frac{1}{4},\frac{1}{4}$	8
T_2 (6l) x,2x,0		6s	0	2	2	T_2 (8i) x,0,0	8
T_3 (2e) 0,0,z		2s	0.44	2s	0.84	T_3 (8j) $x,\frac{1}{2}$,0	8
T_4 (3g) $\frac{1}{2}$,0,$\frac{1}{2}$	3	3	3	3	3		

TABLE III. The relationship between the well known RT_{12} $I4/mmm$ tetragonal sites and the new out-of-equilibrium the $P6/mmm$ hexagonal ones.

Tetragonal		New hexagonal phase
2a(0, 0, z)	$\longrightarrow$	1a(0, 0, 0)
8i (x, 0, 0)	$\longrightarrow$	2e(0, 0, z)
8i (x, 0, 0)	$\longrightarrow$	$\frac{1}{3}$ of 6l(x, 2x, 0)
8j (x, $\frac{1}{2}$, 0)	$\longrightarrow$	$\frac{2}{3}$ of 6l(x, 2x, 0)
8j (x, $\frac{1}{2}$, 0)	$\longrightarrow$	$\frac{1}{3}$ of 3g($\frac{1}{2}$, 0, $\frac{1}{2}$)
8f ($\frac{1}{4}$, $\frac{1}{4}$, $\frac{1}{4}$)	$\longrightarrow$	$\frac{2}{3}$ of 3g($\frac{1}{2}$, 0, $\frac{1}{2}$)

hand, we have shown that the R_B agreement factor get higher and the best one must obviously correspond to the lowest value which is found to be equal to s= 0.42, leading to a 1/10 stoichiometry. In addition, we have maintained the 6l occupancy rates equal to 0.33 to ensure the best geometrical equilibrium among T hexagons. It is worth to note that the obtained samples are single phase (1/12 and 1/10); no residual Sm-Fe phases are detected.

In the fitting procedure, we have taken into account all of the following parameters: a, c, diffraction domain size D, Debye-Waller factors, atom space-group position, and s. Moreover, the relative distribution of the Fe, Mo atoms was assumed according to the distribution in the $ThMn_{12}$ structure and the evolution of the crystallographic family from the hexagonal parent to the tetragonal structure described in table III. The results of the Rietveld analysis relative to the hexagonal $P6/mmm$ type phase are given in table IV for x = 1, 1.5, 2.

The resulting Rietveld refinement of the sample $SmFe_{10.5}Mo_{1.5}$ annealed at 750 °C is shown in figure 6, which displays a good agreement between the measured and calculated profiles as can be seen from the difference curve versus 2θ. The dependence of cell parameters versus x, Mo content, of the hexagonal phase is similar to the corresponding ones of the $SmFe_{12-x}Mo_x$ compounds as shown on table IV.

In order to shed light on the hexagonal phase stoichiometry, Rietveld refinement is performed for a nominal composition while varying the vacancy rate s. The best agreement factor R_B between the calculated and the measured diffraction line intensities is obtained with s=0.42. R_B is systematically increased when the refinement is performed with other s values. For s = 0.5 witch

TABLE IV. Crystallographic parameters from Rietveld refinement of the $P6/mmm$ hexagonal phase annealed at 750°C. a and c unit cell parameters, χ^2, R_B agreement factors and D domain size.

	x = 1	x = 1.5	x = 2
a (Å)	4.879	4.882	4.888
c (Å)	4.241	4.261	4.253
x{6l}	0.282	0.284	0.281
z{2e}	0.285	0.286	0.285
χ^2	4.37	4.35	3.55
R_B	1.92	2.72	2.10
D (nm)	29	34	47

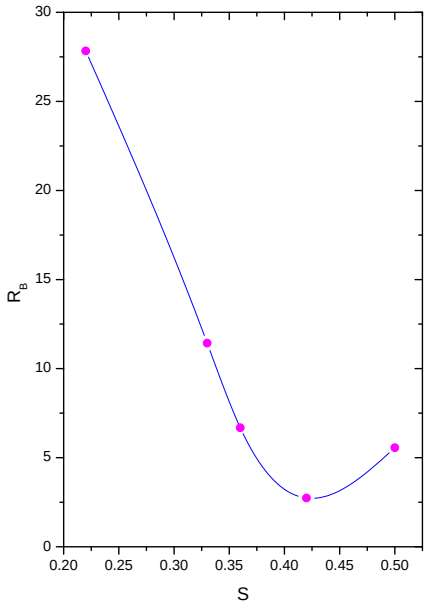

FIG. 7. R_B variation for different s values in the $P6/mmm$ structure.

is relative to the 1/12 stoichiometry R_B is quite higher than 5. The highest R_B is achieved for s=0.22 witch corresponds to the $TbCu_7$, 1/7 stoichiometry. Figure 7 represents the agreement factor variation as a function of the s vacancy rate for the hexagonal phase. The 1/7 ($TbCu_7$) approach is demonstrated to be not pertinent. In fact, the minimum is obtained for $s = 0.42$ which is relevant to a 1/10 stoichiometry. Until this present work, no one has invoked a possible stoichiometry evolution of the $Sm(Fe,Mo)_{10}$ toward $Sm(Fe,Mo)_{12}$ composition.

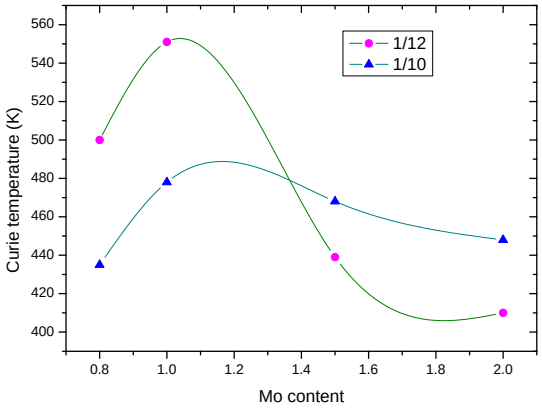

FIG. 8. Curie temperature vs x Mo content.

B. Intrinsic magnetic properties

Intrinsic magnetic properties, were studied for the various samples. Systematic thermomagnetic data were carried out for different Mo content and annealing temperatures.

There are three types of exchange interaction existing in $RFe_{12-x}M_x$ compounds, namely the R-R interaction between the magnetic moments on the R-sublattice, the T-T interaction between the magnetic moments on the T- sublattice, and the R-T intersublattice interaction. Among them, the T-T interaction is the strongest and determines the ordering temperature. It is well known that the T-T interaction is very sensitive to the distance between the transition metal moments. Hu et al.[36] have reported that Fe at the 8i site has the largest magnetic moment while Fe at the 8f site has the smallest moment.

The inter-atomic distances between the neighbors of Fe atoms at the different sites are different. According to Givord and Lemaire[37], there are two T-T exchange interactions in R_2Fe_{17} compounds, positive and negative. When the distance of the Fe-Fe pairs is smaller than 2.45 Å, the exchange interaction is negative; whereas at larger Fe-Fe distances the interaction is positive.

It may be assumed that this is also the case in the 1/12 system. So, when the substitution of Mo for Fe occurs at sites where the distance between Fe-Fe pairs is smaller than a certain critical distance, the negative interaction will be reduced and the total interaction will be enhanced, so that the Curie temperature will increase because of the substitution of Mo for Fe. The decrease of the Curie temperature is due to magnetic dilution. The same tendency trend evolution is observed for the corresponding precursor phases.

As shown in figure 8 the Curie temperature depends on the Mo concentration and increases from 500 to 560 K for the 1/12. The same tendency is obtained for the hexagonal 1/10 new phase, nevertheless, it remains lower than the Curie temperature of the tetragonal 1/12 equilibrium one. Up to a certain Mo amount the out of equilibrium phase shows higher T_C values than the 1/12 one.

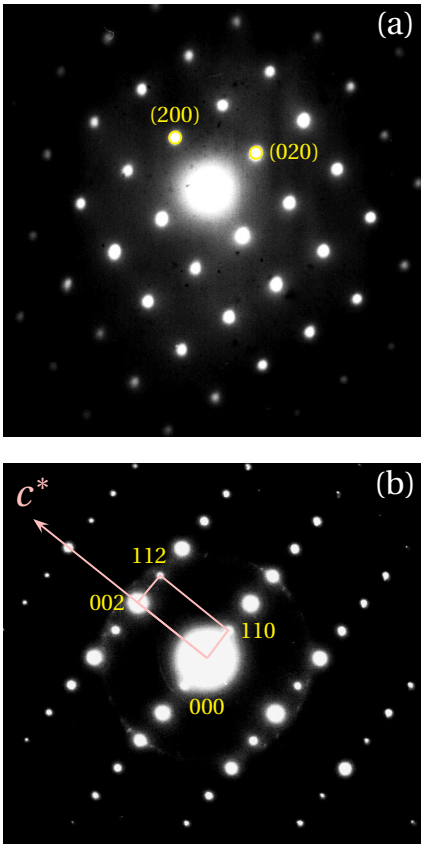

FIG. 9. Selected area diffraction pattern : (a) along $[001]^*$ zone axis, (b) along $[1\bar{1}0]^*$ zone axis, of the tetragonal $SmFe_{11}Mo$ annealed at 1190 °C.

C. Correlation between nanostructure and extrinsic magnetic properties

In order to explore the nanostructure of $Sm(Fe,Mo)_{12}$ alloys, transmission electron microscopy was employed, combined with selected area diffraction (SAED) patterns and microanalysis.

Figure 9 shows the electron diffraction patterns, which

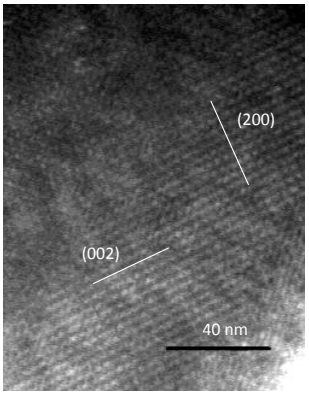

FIG. 10. High-resolution transmission electron microscopy micropgraph of the tetragonal $SmFe_{11}Mo$ annealed at 1190 °C.

can be completely indexed in the tetragonal $ThMn_{12}$ type structure viewed along the [001]* zone axis (Fig. 9a) and along the $[1\bar{1}0]$* zone axis (Fig. 9b).

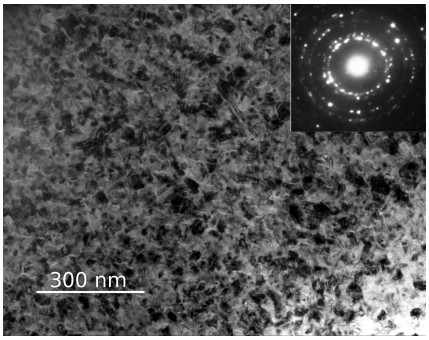

FIG. 11. Transmission electron microscopy micrograph of the the hexagonal $SmFe_9Mo$. Inset : Selected area diffraction pattern.

The corresponding [010] high-resolution transmission electron microscopy image is presented in figure 10, the different lattice plans can be identified as (002) and (200) of the 1/12 equilibrium phase.

Figures 11 and 12 show the corresponding bright field image of the hexagonal $SmFe_9Mo$ and grain size distribution of the 1/10 out of equilibrium phase. The selected area diffraction pattern shown in Figure 11 (inset) displays a polycrystalline ring feature, because of the presence of many nanocrystals within the selective aperture.

The grain size ranges from 25 to 50 nm. Note that the diffracted crystallite size calculated from the XRD technique gives an average crystallite size over a large area of the sample while TEM results are based on the average size of a limited amount of grains.

The hysteresis loop of $SmFe_{10.5}Mo_{1.5}$ annealed at 850 °C (Fig. 13) shows that, the remanence, $M_R = 42$emu/g and the remanence ratio $M_R/M_S = 0{,}59$ inherent to nanocrystalline state[38–40], as confirmed by transmission electron microscopy.

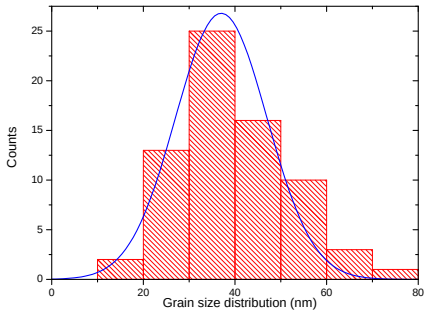

FIG. 12. Grain size distribution for the hexagonal $SmFe_9Mo$

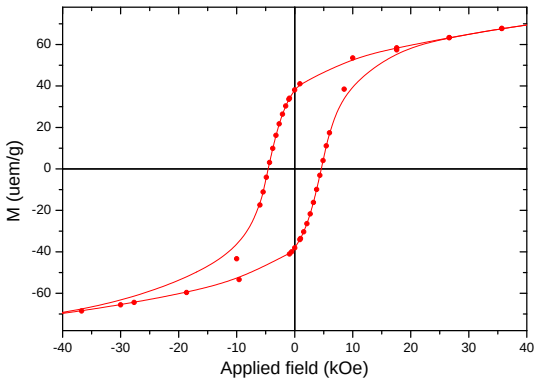

FIG. 13. Hysteresis loop of $SmFe_9Mo$.

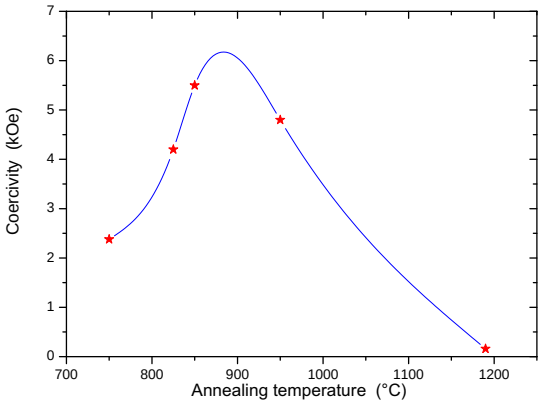

FIG. 14. Coercivity vs annealing temperature.

Fig. 14 shows the dependence of the coercive field on annealing temperature. The evolution of the coercivity suggests two different regimes. H_C increases up to 5.5 kOe when T_a=850 °C then decreases. Let's note that coercivity is not an intrinsic magnetic property; as a result the coercive field value as well as the magnetization reversal process depends not only on the chemical composition, the temperature and the magnetic anisotropy, but also strongly to the microstructure[41]. For low annealing temperature, the sample often has many defects[23,38]

resulting from high energy milling and in that case crystallite sizes are very small. This leads to low values of coercivity. It is well known that the auto-coherent domain size increases with T_a[23]. So, at T_a=850 °C, one can say that the grain size is of the desired optimal diameter.

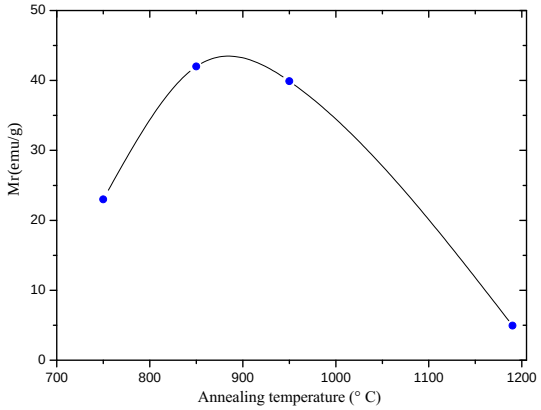

FIG. 15. Remanence vs annealing temperature.

Furthermore, the critical single domain diameter, D_c, of the two phases can be estimated from the equation: $D_c = \frac{9\gamma}{2\pi M_s^2}$, where γ is the domain energy wall. It is around 67 nm for the 1/10 phase and 85 nm for the 1/12 one. So, whatever the used annealing temperature, we are always below the single domain size. Then, the decrease of H_C at high T_a might be due to an unsustainable microstructure.

The same trend evolution for the remanence vs temperature is observed (Fig. 15)

IV. CONCLUSIONS

(i) High energy ball milling and subsequent annealing at $T_A > 900$ °C leads to a continuous and homogeneous substitution of Mo for Fe in the $I4/mmm$ $SmFe_{11}Mo$ compound. The unit cell parameters a and c increase upon Mo substitution.

(ii) For $T_A < 800$ °C an hexagonal $P6/mmm$ $CaCu_5$-type phase, precursor of the $I4/mmm$ $SmFe_{12-x}Mo_x$ phase, is detected as the main phase. The Rietveld analysis gives a phase stoichiometry 1/10, with three crystallographic transition metals sites 2 ($6l$) atoms, 3 ($3g$) atoms, $2s$ ($2e$) and one Sm site $1-s$ ($1a$).

(iii) For $850 < T_A < 1190$ °C the hexagonal phase transforms into the tetragonal phase.

(iv) Coercivity exhibits two antagonist behaviors as a function of annealing temperature T_A. When increasing T_A, on the one hand, the number of surface defects is reduced, it results in an increase of H_C, on the other hand, the diffraction auto-coherent domain size increases which reduces H_C. The intersection of both behaviors occurs around 850 °C where H_C shows a maximum. The high H_C value up to 5.5 kOe suggests that such samples are potential candidates for magnetic recording media and eventually permanent magnets.

V. ACKNOWLEDGMENTS

This work was main supported by the CNRS and the "Ministère de l'Enseignement Supérieur, de la Recherche Scientifique" (LAB MA03) (Tunisia).

The authors acknowledge the French-Tunisian Cooperation PHC-Utique (project 11/G 1301).

The authors acknowledge Véronique Charbonnier for the technical help.

[1] M. Sagawa, S. Fujimara, N. Togawa, H. Yamamoto, and Y. Matsuara, J. Appl. Phys. **55**, 2083 (1984).
[2] D. B. de Mooij and K. H. Buschow, J. Less-Common. Met. **136**, 207 (1988).
[3] R. Verhoef, F. de Boer, Z. Zhi-dong, and K. Buschow, J. Magn. Magn. Mater. **75**, 319 (1988).
[4] Q. F. Xiao, Z. D. Zhang, T. Zhao, W. Liu, Y. C. Sui, X. G. Zhao, and D. Y. Geng, J. Appl. Phys. **82**, 6170 (1997).
[5] L. Bessais, S. Sab, C. Djega-Mariadassou, and J. M. Greneche, Phys. Rev. B **66**, 54430 (2002).
[6] Y. Z. Wang, B. P. Hu, G. C. Liu, J. H. Hu, L. Son, K. Y. Wang, and W. Y. Lai, J. Appl. Phys. **76**, 6383 (1994).
[7] K. H. J. Buschow, J. Less-Common. Met. **144**, 65 (1988).
[8] F. R. D. Boer, Y. K. Huang, D. B. D. Mooij, and K. H. J. Buschow, J. Less-Common. Met. **135**, 199 (1987).
[9] K. H. J. Buschow, J. Magn. Magn. Mater. **100**, 79 (1991).
[10] H. Pan, J. Magn. Magn. Mater. **184**, 365 (1998).
[11] K. Ohashi, T. Yokoyama, R. Osugi, , and Y. Tawara, IEEE Trans. Magn. Mag. **MAG-23**, 3101 (1987).
[12] H. Saito, M. Takahashi, and T. Wakiyama, J. Appl. Phys. **64**, 5965 (1988).
[13] W. Kaiying, H. Jifan, W. Yizhong, H. Boping, and W. Zhenxin, Phys. Status Solidi (A) **148**, K29 (1995).
[14] S. Khazzan, N. Mliki, L. Bessais, and C. Djega, J. Magn. Magn. Mater. **322**, 224 (2010).
[15] L. Bessais, C. Djega-Mariadassou, A. Nandra, M. D. Appay, and E. Burzo, Phys. Rev. B **69**, 064402 (2004).
[16] L. Bessais, E. Dorolti, and C. Djega-Mariadassou, Appl. Phys. Lett. **87**, 192503 (2005).
[17] L. Schultz, K. Schnitzke, and J. Wecker, J. Magn. Magn. Mater. **83**, 254 (1990).
[18] L. Wei, W. Qun, X. K. Sun, X. G. Zhao, T. Zhao, Z. D. Zhang, and Y. C. Chuang, J. Magn. Magn. Mater. **131**, 413 (1994).
[19] L. Bessais, S. Sab, C. Djega-Mariadassou, N. H. Dan, and N. X. Phuc, Phys. Rev. B **70**, 134401 (2004).
[20] S. F. Cheng, V. K. Sinha, Y. Xu, J. M. Elbicki, E. B. Boltich, W. E. Wallace, S. G. Sankar, and D. E. Laughlin, J. Magn. Magn. Mater. **75**, 330 (1988).
[21] J. Rodríguez-Carvajal, Physica B **192**, 55 (1993).
[22] L. Bessais, E. Dorolti, and C. Djega-Mariadassou, J. Phys.: Condens. Matter **18**, 3845 (2006).
[23] S. Khazzan, N. Mliki, and L. Bessais, J. Appl. Phys. **105**, 103904 (2009).
[24] L. Bessais and C. Djega-Mariadassou, Phys. Rev. B **63**, 54412 (2001).
[25] Z. W. Li, X. Z. Zhou, and A. H. Morrish, J. Appl. Phys. **69**, 5602 (1991).

[26]H. Sun, Y. Morri, H. Fujii, M. Akayama, and S. Funahashi, Phys. Rev. B **48**, 13333 (1993).
[27]Z. Hu, W. B. Yelon, X. Zhang, and W. J. James, J. Appl. Phys. **79**, 5522 (1996).
[28]Z. X. Tang, E. W. Singleton, and G. C. Hadjipanayis, J. Appl. Phys. **73**, 6254 (1993).
[29]A. Teresiak, M. Kubis, N. Mattern, M. Wolf, and K.-H. Muller, J. Alloys Compd. **274**, 284 (1998).
[30]L. Bessais, C. Djega-Mariadassou, H. Lassri, and N. Mliki, J. Appl. Phys. **106**, 103904 (2009).
[31]H. R. Kirchmayer and E. Burzo, Landolt-Börnstein : Crystal and Solid State Physics, Numerical Data and Functional Relationships in Science and Technology, Vol. 19, 250 (Spinger-Verlag, Berlin, 1990).
[32]R. Fischer, T. Schrefl, H. Kronmuller, and J. Fidler, J. Magn. Magn. Mater. **153**, 35 (1996).
[33]D. Givord, J. Laforest, J. Schweizer, and F. Tasset, J. Appl. Phys. **50**, 2008 (1979).
[34]C. Djega-Mariadassou and L. Bessais, J. Magn. Magn. Mater. **210**, 81 (2000).
[35]A. Teresiak, O. Gutfleisch, N. Mattern, B. Gebel, and K.-H. Muller, J. Alloys Compd. **346**, 235 (2002).
[36]B. Hu, K. Wang, Y. Wang, Z. Wang, Q. Yan, and X. Sun, Phys. Rev. B **51**, 2905 (1995).
[37]D. Givord and R. Lemaire, IEEE Trans. Magn. Mag. **MAG-10**, 109 (1974).
[38]E. F. Kneller and R. Hawig, IEEE Trans. Magn. Mag. **27**, 3588 (1991).
[39]D. L. Leslie-Pelecky and R. L. Schalek, Phys. Rev. B **59**, 457 (1999).
[40]J. X. Zhang, L. Bessais, C. Djega-Mariadassou, E. Leroy, A. Percheron-Guegan, and Y. Champion, Appl. Phys. Lett. **80**, 1960 (2002).
[41]D. Givord and M. R. ans V. M.T S. Barthem, J. Magn. Magn. Mater. **258**, 1 (2003).